ACS Macro Letters

pubs.acs.org/macroletters Letter

Fast Fabrication of Porous Amphiphilic Polyamides via Nonconventional Evaporation Induced Phase Separation

Tao Wen,* Yuting Gao, Jiajia Zhou, Jie Qiu, Shuo Wang, Joachim Loos, Dujin Wang, and Xia Dong*

Cite This: ACS Macro Lett. 2023, 12, 697−702 Read Online

ACCESS | Metrics & More | Article Recommendations | Supporting Information

ABSTRACT: In the present work, we report a facile approach for the fast fabrication of porous films and coatings of long-chain polyamides through a nonconventional evaporation induced phase separation. Because of its amphiphilic nature, polyamide 12 can be dissolved in the mixture of a high-polarity solvent and a low-polarity solvent, while it could not be dissolved in either solvent solely. The sequential and fast evaporation of the solvents leads to the formation of porous structures within 1 min. Moreover, we have investigated the dependence of the pore structures on composition of the solutions, and have demonstrated that our approach can be applied to other long-chain polycondensates, too. Our findings can provide insight on the fabrication of porous materials by using amphiphilic polymers.

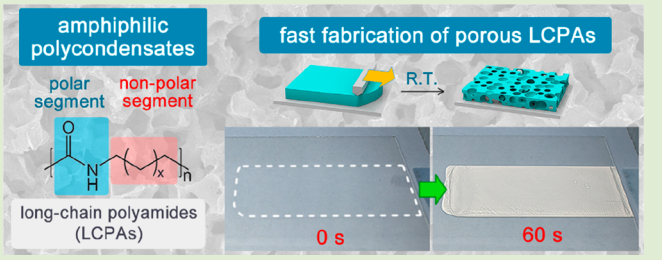

Polymer-based porous materials have attracted increasing attention in the past decades because of their enormous potentials in the applications of separation, catalysis, energy storage, and conversion.[1−7] Various techniques have been developed to fabricate porous polymer materials, while phase separation (or phase inversion) is the most important approach due to its high efficiency and low cost.[8−10] For example, most of the commercial polymer membranes are prepared by using nonsolvent induced phase separation (NIPS), thermally induced phase separation (TIPS), or evaporation induced phase separation (EIPS).[11−16] Generally, high-boiling-point solvents like dimethylformamide or *N*-methyl pyrrolidone and coagulation baths are commonly utilized for these fabrication processes.[10] Therefore, high-temperature baking is needed to accelerate the evaporation of the solvents. Moreover, it is difficult to separate the high-boiling-point solvents from H_2O, which usually is used as a poor solvent, so additional economic costs are involved to recycle the liquid solvent waste. In fact, fast fabrication of porous polymer materials is required to meet the increased demands in some cutting-edge applications, such as passive daytime radiative cooling,[17] acoustic absorption,[18] antireflection coatings,[19] slippery lubricant-infused porous surfaces (SLIPS),[20] etc.

All the phase-separation-based methods exploit the dissolution and precipitation of polymers in solvents. From a thermodynamic point of view, the dissolution and precipitation of polymers in the given solvents are governed by the interactions between the solvents and the polymers, including dispersive interactions, polar cohesive forces, and hydrogen bonding.[21] When the interchain attractive force of a polymer is similar to that of a solvent, the polymer is expected to be dissolved in that solvent.[22−24] According to this basic principle, an amphiphilic polymer consisting of high-polarity and low-polarity segments (i.e., amphiphilic) is expected to be dissolved by a mixture of high-polarity solvent (S_H) and low-polarity solvent (S_L), even when both are nonsolvents for the polymer.[22] Due to the different evaporation rates of the two solvents, sequential evaporation can shift the solubility of the mixed solvents, leading to phase separation (Scheme 1a). Note that S_L usually possesses a faster evaporation rate than S_H due to its lower cohesive energy.

Long-chain polycondensates (LCPCs) are a family of polycondensates containing long aliphatic segments $-(CH_2)_n-$ ($n \geq 10$), for instance, long-chain polyamides (LCPAs), long-chain polyurethanes (LCPUs), and long-chain polyureas (LCPUAs).[25,26] These macromolecules combine the molecular architecture of conventional polyolefins and polycondensates and have great potential in pursuing green bioplastics by using renewable natural resources.[26,27] In particular, the alternating arranged amide bonds (or urethane bonds, urea bonds, etc.) and long alkyl chain segments along the backbones endow LCPCs with amphiphilic feature.[23,27] In this work, we report an approach for fast fabrication of porous LCPCs through a nonconventional EIPS. We have employed polyamide 12 (PA12) as a model polymer. PA12 can be

Received: February 13, 2023
Accepted: May 10, 2023

https://doi.org/10.1021/acsmacrolett.3c00086
ACS Macro Lett. 2023, 12, 697−702

Scheme 1. (a) Illustration of Dissolution and Precipitation of the Amphiphilic Polymer with Alternating Polar and Nonpolar Segments along Their Backbone in the Mixed Solvent; (b) PA12 Containing Polar Amide Groups and Nonpolar Alkyl Chain Segments Can Be Dissolved in the Mixture of S_H and S_L, and a Porous PA12 Film is Formed after Sequential Evaporation of the Solvents

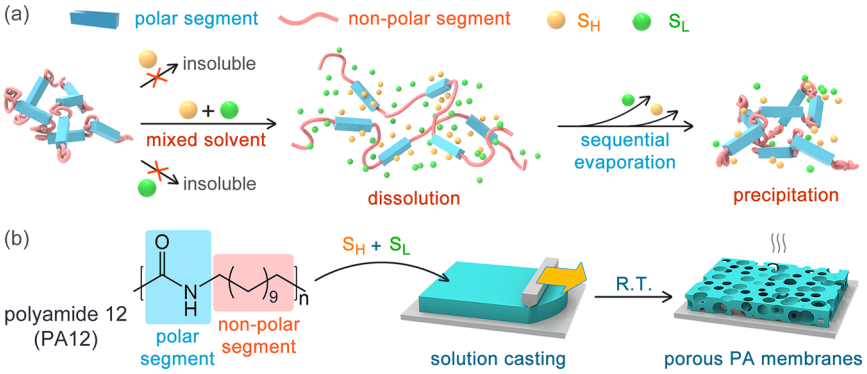

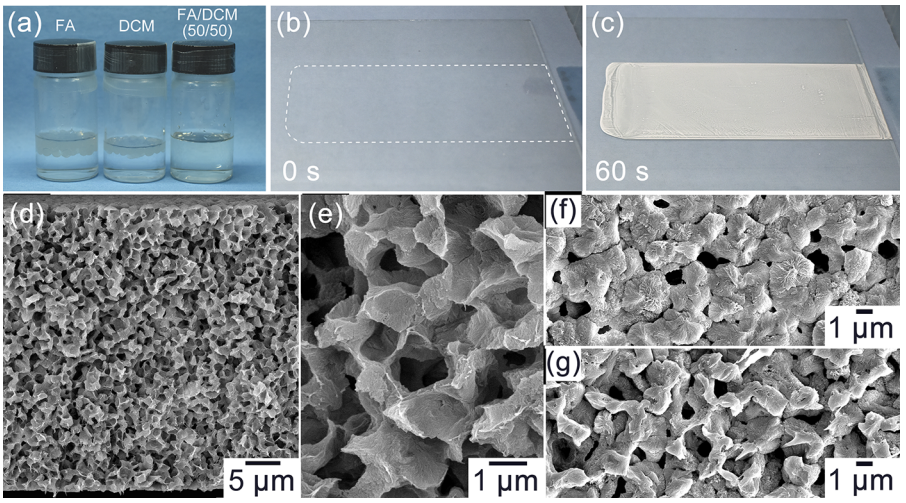

Figure 1. Photograph of PA12 pellets kept in FA, DCM, and the mixture of FA/DCM (f_{FA}: 50%) overnight (a). Photographs of the as-casted PA12 wet film (b) and the casted PA12 film dried at ambient condition for 60 s (c). Cross-sectional SEM micrographs of a porous PA12 film at low and high magnification (d, e). SEM micrographs of the top surface (f) and bottom surface (g) of a PA12 film (w_{PA}: 11.5%, f_{FA}: 50%).

dissolved in a mixture of formic acid (FA) and dichloromethane (DCM), and porous structures of PA12 with homogeneous pore size distributions can be prepared through the evaporation of the solvents after solution casting (Scheme 1b). Because of the low boiling points of the mixed solvents, vitrification and pore-formation can be accomplished within 1 min. By taking advantage of the high volatility of FA and DCM and the large difference in their boiling points, the solvents could be recycled straightforwardly through a low energy-consuming process. This work may develop a new route to fabricate porous membranes and coatings with amphiphilic polymers.

We start our study with investigating the dissolution behavior of PA12. Due to the amphiphilic nature of PA12, it is resistant to the most commonly used solvents, including strong acids and strong oxidizing agents. According to the previous report by Gogotsi and co-workers,[23] FA and DCM are selected as the S_H and S_L, respectively. Note that FA and DCM are miscible at arbitrary ratios. As shown in Figure 1a, PA12 pellets were not dissolved or swollen in DCM, whereas they were only slightly swollen in FA at room temperature for the LCPA concentration, i.e., weight fraction, $w_{PA} = m_{PA}/(m_{PA} + m_{FA} + m_{DCM})$, of 11.5%. In contrast, PA12 can be completely dissolved in the mixture of FA and DCM after several hours at room temperature with the FA weight fraction of 50% in the mixed solvent, $f_{FA} = m_{FA}/(m_{FA} + m_{DCM})$. This observation is consistent with the previous report.[23] It is noteworthy that PAs with short hydrocarbon chain segments, such as PA6 and PA66, are fully dissolvable in pure FA (Figure S1), demonstrating that the immiscibility of PA12 in FA is due to the presence of the long alkyl chains. The solubility of polymers in a given solvent can be described by Hansen solubility parameters.[22] Figure S2 shows the Teas graph of PA12, FA, and DCM. It is observed that the point with respect to PA12 is located at the line connecting the FA and DCM points, confirming that the mixture of FA and DCM with proper ratio can act as a good solvent for PA12. This result agrees well with the above observation.

We have blade-coated PA12 solution (w_{PA}: 12.3%, f_{FA}: 50%) on a glass plate at ambient condition, and subsequently investigated the solidified film. The as-cast wet film was transparent, and it rapidly changed to a white opaque appearance within 60 s (Figures 1b and 1c, Movie S1). This observation implies the occurrence of phase separation in the film during solvent evaporation. To confirm the microscopic structure of the dried PA12 film, scanning electron microscope

https://doi.org/10.1021/acsmacrolett.3c00086
ACS Macro Lett. 2023, 12, 697−702

(SEM) observation was conducted. Figure 1d shows the cross-sectional SEM micrograph of a PA12 membrane, in which pores with homogeneous sizes of approximately 1 μm are observed. The interconnected cellular pore structure clearly is seen by high magnification SEM observations (Figure 1e). Figure 1f and g show SEM micrographs of the top and bottom surfaces of the PA12 film, respectively. The top surface of the PA12 film exhibits a "skin" structure with nodule-like appearance, potentially of spherulitic superstructures, whereas the bottom surface shows a continuous network-like morphology. Based on the above morphological observations, the formation of porous structures in dried PA12 is mainly attributed to liquid−liquid phase separation induced by solvent evaporation.[8] The morphology of the free surface is ascribed to the crystallization of PA12, whereas the network-like morphology at the bottom is due to the direct nucleation of PA12 on the glass surface. Similar morphologies are observed in short-chain polyamide membranes prepared by traditional NIPS.[28] For comparison, we have prepared casted films of PA6 and PA66 from the mixed FA/DCM solvent (f_{FA}: 50%), in which packed spherical structures with sizes larger than 10 μm are observed (Figure S3).

The above shown results indicate that the evaporation of mixed solvents induces pore formation in PA12. To further investigate the mechanism of phase separation in long-chain PAs, the theoretical phase diagram of LCPAs in the mixed solvent was investigated. Briefly, we introduced an ideal alternating copolymer model consisting of two monomers, i.e., C and D, and degree of polymerization is N_P. Two solvents, A and B, are only preferred to a single monomer species, namely, A can dissolve C but not D, and B can dissolve D but not C. The Flory−Huggins free energy is determined by the volume fraction (f_C and f_D) and the interaction parameters (χ_{AC}, χ_{BD}, χ_{AD}, and χ_{BC}). The phase diagram is constructed using the convex hull construction (see details in SI).[29] Figure 2a shows the theoretical ternary phase diagram of CD/A/B, in which two separated binodal lines can be found as $\chi_{AD} = \chi_{BC} = 1.8$. Interestingly, merging of the two binodal lines takes place when χ_{AD} and χ_{BC} increase to 2.0, enclosing a region close to the coordinate axis of both solvents A and B (Figure 2b). It revealed that, in the ternary system of an amphiphilic polymer and two nonsolvents, two binodal lines are present in the phase diagram. The strong interactions of polymer and preferred solvents can induce the merging of the two binodal lines, and the merged binodal lines create a region with the coordinate axis of the two solvents, which represents the single-phase region in the phase diagram (see below).

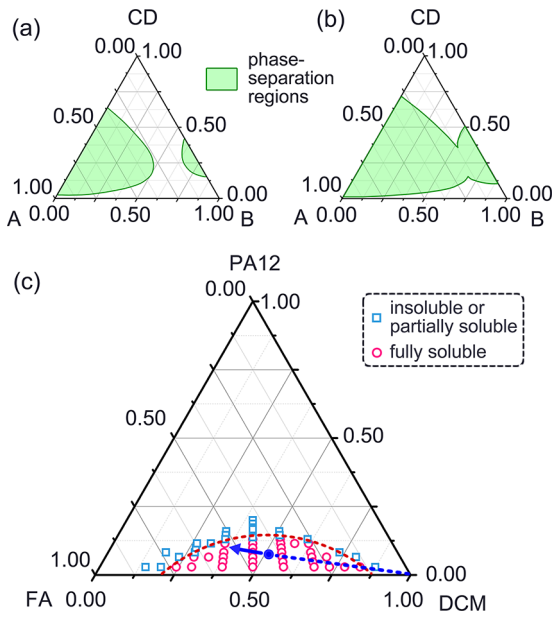

Figure 2. (a, b) Calculated ternary phase diagrams of copolymer CD in the mixed solvent of A and B. The solid green lines represent the binodal lines. (b) $N_P = 10$, $f_C = 0.4$, $\chi_{CD} = 0$, $\chi_{AD} = \chi_{BC} = 1.8$; (c) $N_P = 10$, $f_C = 0.4$, $\chi_{CD} = 0$, $\chi_{AD} = \chi_{BC} = 2.0$. (c) The experimental ternary phase diagram of PA12 in the mixed solvents FA and DCM.

Further, we have investigated the experimental phase diagram of PA12/FA/DCM. As both FA and DCM are poor or nonsolvents for PA12, we are unable to apply the standard cloud-point method[30] to plot the phase diagram. Instead, the solubilities of PA12 with respect to f_{FA} and w_{PA} were determined. Figure 2c shows the ternary phase diagram of PA12 mixed with FA and DCM, which is established experimentally at room temperature. According to the solubility of PA12 in the mixed solvents, the boundary between the soluble region and the insoluble/partially soluble region is determined and indicated by the red dashed line in Figure 2c. Note that this boundary is not the binodal curve. The location of the soluble region (or single-phase region) in Figure 2c is defined by the phase boundary and the coordinate axis of the two solvents, which is different from the typical phase diagrams in conventional NIPS and EIPS systems.[15,31]

Based on the theoretical and experimental phase diagrams, we are able to uncover the generation mechanism of the porous structures of PA12 during the evaporation of the mixed solvents. Due to the amphipathic nature of long-chain PAs, PA12 can be fully dissolved in the mixture of FA and DCM. On the ternary phase diagram, the initial solution composition is located in the homogeneous region (solid blue spot in Figure 2c). After coating the solution onto the substrate, the mixed solvents start to evaporate. The evaporation rate of DCM is about 30 times faster than the one of FA at ambient temperature (Figure S4a), therefore the evaporation of FA can be omitted in the initial stage. In this case, the composition of the wet film changes nearly straight along the line joining the vertex and the initial composition point (blue dashed line and arrow in Figure 2c), and the phase separation occurs when the path of composition crosses the phase boundary. The formation of continuous pores, rather than dispersed droplet-like structures, suggests the occurrence of spinodal decomposition during fast solvent evaporation.[32] Moreover, it is noteworthy to mention that the evaporation rate of FA is about 60 times faster than the one of H_2O at an humidity of 78% (Figure S4b). Therefore, we expected that the fabrication process introduced in our study is substantially faster than the conventional approach using H_2O as the poor- or nonsolvent.

We have investigated the morphological dependence of the porous PA12 films on f_{FA} and w_{PA}. Figure 3a−d shows the representative SEM micrographs of porous PA12 films prepared with different w_{PA} and f_{FA}; corresponding initial PA12 concentrations in the solutions are marked in the phase diagram of Figure 3e. As the value of w_{PA} is above 9%, homogeneous pore sizes are seen through the whole thickness (Figures 3a,b, S5, and S6). However, when the polymer concentration is reduced to 7.4%, the film exhibited of a collapsed structure (Figure S5e). The surface morphologies of PA12 films prepared with different w_{PA} are observed, too

https://doi.org/10.1021/acsmacrolett.3c00086
ACS Macro Lett. 2023, 12, 697−702

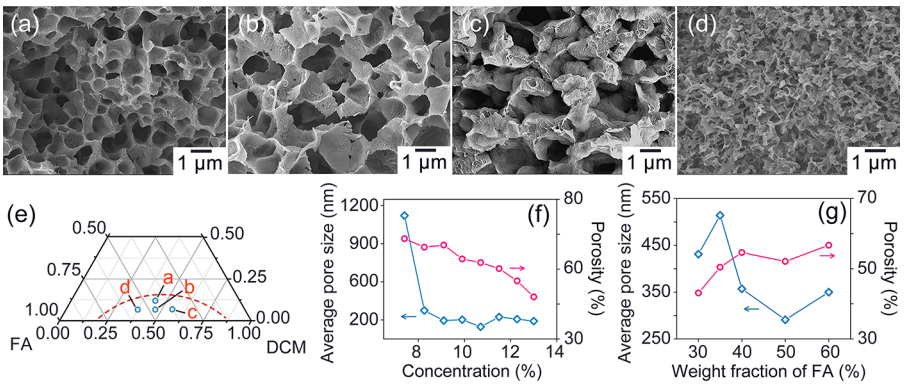

Figure 3. (a–d) Cross-sectional SEM micrographs of porous PA12 films prepared with different values of w_{PA} and f_{FA}, and the corresponding initial compositions of the PA12 solutions (e). (a) w_{PA}: 11.5%, f_{FA}: 50%; (b) w_{PA}: 8.2%, f_{FA}: 50%; (c) w_{PA}: 8.2%, f_{FA}: 30%; (d) w_{PA}: 8.2%, f_{FA}: 60%. Dependence of the average pore sizes and porosities of the PA12 films on w_{PA} (f) and f_{FA} (g).

(Figures S7 and S8). A thin dense layer with some pores having sizes of ~1 μm is observed, whereas the bottom surfaces of PA films exhibit pores with dominant sizes of 1–3 μm. To gain quantitative information on the porosity of the PA12 films, the average pore sizes were measured by a capillary flow porometer. Note that the pore sizes measured by the capillary flow porometer reflect the dimension of the constrained part of the pores, i.e., the pore throat.[33] Figure 3f shows the dependence of average pore sizes of the PA12 films on the value of w_{PA}. Besides the sample prepared with a solution concentration of 7.4%, the average pore sizes are around 200 nm. Moreover, the porosities decreases with increasing PA12 concentration in the casting solution from 68% to 52%.

Next, we have examined the dependence of the morphology on the compositions of the mixed solvents. Figure 3c,d shows the cross-sectional SEM micrographs of porous PA12 membranes prepared from casting solutions with different f_{FA} for constant w_{PA} of 8.2%. For all samples, homogeneous porous structures are seen (Figure S9). However, the morphologies of the pores have obviously changed with the variation of f_{FA}. The porous PA12 film prepared with f_{FA} of 35% exhibited cellular pores (Figure 3c). As f_{FA} is reduced to 30%, the porous PA12 film shows a more compact structure with interconnecting morphology (Figure 3d). It is found that the average pore size changed with the value of f_{FA}, however, it did not follow a linear relation (Figure 3g). Roughly speaking, a higher value of f_{FA} gives smaller pore sizes. Probably, the smaller pore sizes are caused by the relative lower evaporation rates of the mixed solvent for such higher f_{FA} concentrations.

To address this hypothesis, we have prepared a PA12 film by slow solvent evaporation, i.e., by keeping the as-cast film in a sealed box. We have found that the pore morphology of this membrane is similar to the one shown in Figure 3d (Figure S10), confirming that slow solvent evaporation could decrease the pore size. It is noteworthy to mention that FA is able to dissolve PA12 at high temperature, indicating that FA is not a strictly non- or poor solvent. We speculate that, with a high f_{FA}, the evaporation of DCM from the liquid medium will give a shallow quench with respect to the binodal line.[34] As a result, the crystallization of PA12 would possess a compact structure in the concentrated wet films.[35] Corresponding DSC results indicate that the melting enthalpies of the PA12 membranes are almost independent of f_{FA} (Figure S11), which means that the morphological differences of the PA12 films most probably are not caused by differences of their crystallization behavior.

The above shown results demonstrate that porous membranes of PA12 can be fabricated through a facile and fast process. We believe that our method is applicable to other LCPAs, too. Therefore, we have prepared cast films of PA1012, PA612, and PA610 applying the same process. For PA1012 and PA612 cast-films, a homogeneous porous morphology is seen very similar to the PA12 membrane morphology (Figure S12a,b), whereas for PA610 films a morphology of irregular pores with sizes of ~5 μm is seen (Figure S12c). We speculate that the latter is caused by the high amide segment frequency of PA610 (1/9) and thus its relatively higher solubility in FA compared to PA12, PA1012, and PA612. For such a case, the slow precipitation of the polymer may give rise to a denser structure.

Besides investigating the formation of porous LCPA films, we have applied the same solidification approach to long-chain polyurethane, i.e., PU612, and polyurea, i.e., PUA612 (Scheme S1). We have found that porous structures can be obtained in PU612 films (Figure S12d), but only densely packed spheres with irregular pores are found in PUA612 films (Figure S12e). The morphological difference for PUA612 films might be caused by its low solubility in the mixed FA/DMC solution, which results from the strong hydrogen bonds in PUA. Further work is ongoing to better understand membrane formation for PUs and PUAs film-casted from mixed solvents.

Our results reveal that the approach developed in our study potentially is universal for different types of LCPCs. Moreover, it indicates that the membrane morphologies, porosities and pore sizes depend on the synergy of several factors, for instance, the strength of the hydrogen bonding, the length of the alkyl chains, and the components of the mixed solvents.

Furthermore, taking advantage of the fast solvent evaporation and free coagulation bath, our approach not only can be applied to prepare free-standing porous membranes, but also provides a pathway to fabricate porous coating layers onto various substrates, even with complex architectures. Figure 4a,b shows the photographs of metallic keys and screws before and after dip-coating in PA12 solution. It is found that the white coating layer evenly is covering the surfaces of the objects. Further, a wood block with rough surface can be well coated by a PA12 layer, too (Figure 4c). Moreover, we have prepared a 3D-printed model with a double-gyroid network structure by using commercial poly(L-lactide) (PLLA) filaments. This

https://doi.org/10.1021/acsmacrolett.3c00086
ACS Macro Lett. 2023, 12, 697–702

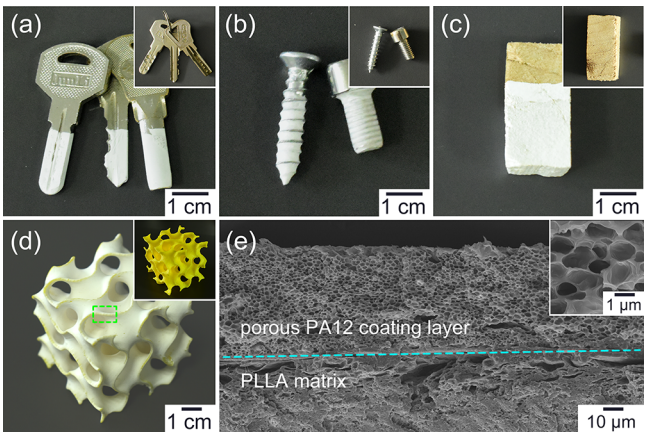

Figure 4. (a–d) Photographs of metallic keys, screws, wood, and 3D-printed double gyroid model before and after coating with PA12 porous layers. (e) Cross-sectional SEM micrographs of the 3D-printed model coated with a PA12 porous layers.

model can be fully coated by immersing it into the PA12 solution. After drying, a uniform PA12 layer is formed on all surfaces (Figure 4d). Figure 4e shows the cross-sectional SEM micrograph of the PA12-coated 3D-printed model, in which a homogeneous porous layer with pore sizes of ∼1 μm is observed. The SEM image shows a homogeneous interface of the PA12 coating with the PLLA substrate, which indicates good adhesion. Moreover, simple scratching of the PA12 coating on PLLA and wood substrates does not remove the coating. On the other hand, adhesion of the coating on the metal key appears substantially weaker. This demonstrates that, besides free-standing membranes, our approach can be employed for fabrication of porous coatings of LCPCs, as well.

In summary, we have introduced a method for fast preparation of porous LCPCs membranes and coatings. Due to its amphiphilic nature, PA12 can be dissolved by the mixture of FA and DCM at room temperature, which both solely are nonsolvents for PA12. The faster evaporation of DCM in the mixed FA/DMC solvents leads to the phase separation of PA12, and in membranes and coatings an homogeneous cellular pore morphology is formed. Taking advantage of the fast evaporation rates of both solvents, the solidification process can be finished within 1 min. The pore sizes and the porosities of PA12 can be tuned by the compositions of the solution. Moreover, we have prepared porous PA1012 and PA612 cast-films applying the same method, and we have demonstrated its feasibility for LCPUs and LCPUAs. This work provides new insight into the development of porous amphiphilic polymer structures and introduces a versatile method for the fast fabrication of porous films and coatings.

■ ASSOCIATED CONTENT

Supporting Information

The Supporting Information is available free of charge at https://pubs.acs.org/doi/10.1021/acsmacrolett.3c00086.

Experimental methods and determination of calculated phase diagram; Additional SEM and DSC results (PDF)

Video of the fast drying process of the film (MP4)

■ AUTHOR INFORMATION

Corresponding Authors

Tao Wen − *South China Advanced Institute for Soft Matter Science and Technology, School of Emergent Soft Matter, South China University of Technology, Guangzhou, China 510640; Guangdong Provincial Key Laboratory of Functional and Intelligent Hybrid Materials and Devices, South China University of Technology, Guangzhou, China 510640;* orcid.org/0000-0002-8376-0608; Email: twen@scut.edu.cn

Xia Dong − *Beijing National Laboratory for Molecular Sciences, CAS Key Laboratory of Engineering Plastics, Institute of Chemistry, Chinese Academy of Sciences, Beijing, China 100190;* orcid.org/0000-0002-6409-7011; Email: xiadong@iccas.ac.cn

Authors

Yuting Gao − *South China Advanced Institute for Soft Matter Science and Technology, School of Emergent Soft Matter, South China University of Technology, Guangzhou, China 510640; Guangdong Provincial Key Laboratory of Functional and Intelligent Hybrid Materials and Devices, South China University of Technology, Guangzhou, China 510640*

Jiajia Zhou − *South China Advanced Institute for Soft Matter Science and Technology, School of Emergent Soft Matter, South China University of Technology, Guangzhou, China 510640; Guangdong Provincial Key Laboratory of Functional and Intelligent Hybrid Materials and Devices, South China University of Technology, Guangzhou, China 510640;* orcid.org/0000-0002-2258-6757

Jie Qiu − *South China Advanced Institute for Soft Matter Science and Technology, School of Emergent Soft Matter, South China University of Technology, Guangzhou, China 510640; Guangdong Provincial Key Laboratory of Functional and Intelligent Hybrid Materials and Devices, South China University of Technology, Guangzhou, China 510640*

Shuo Wang − *South China Advanced Institute for Soft Matter Science and Technology, School of Emergent Soft Matter, South China University of Technology, Guangzhou, China 510640; Guangdong Provincial Key Laboratory of Functional and Intelligent Hybrid Materials and Devices, South China University of Technology, Guangzhou, China 510640*

Joachim Loos − *South China Advanced Institute for Soft Matter Science and Technology, School of Emergent Soft Matter, South China University of Technology, Guangzhou, China 510640; Guangdong Provincial Key Laboratory of Functional and Intelligent Hybrid Materials and Devices, South China University of Technology, Guangzhou, China 510640*

Dujin Wang − *Beijing National Laboratory for Molecular Sciences, CAS Key Laboratory of Engineering Plastics, Institute of Chemistry, Chinese Academy of Sciences, Beijing, China 100190;* orcid.org/0000-0002-2063-0873

Complete contact information is available at: https://pubs.acs.org/10.1021/acsmacrolett.3c00086

Author Contributions

CRediT: **Tao Wen** conceptualization (lead), methodology (lead), project administration (lead), resources (lead), writing-original draft (lead); **Yuting Gao** investigation (lead); **Jiajia**

https://doi.org/10.1021/acsmacrolett.3c00086
ACS Macro Lett. 2023, 12, 697−702

Zhou software (lead), visualization (lead), writing-review & editing (supporting); **Jie Qiu** investigation (supporting); **Shuo Wang** investigation (supporting); **Joachim Loos** writing-review & editing (supporting); **Dujin Wang** supervision (supporting), writing-review & editing (supporting); **Xia Dong** supervision (supporting), writing-review & editing (supporting).

Notes

The authors declare no competing financial interest.

■ ACKNOWLEDGMENTS

We acknowledge the support from the National Natural Science Foundation of China (51890871, U1832220). This work is supported by the Natural Science Foundation of Guangdong (2021A1515010087, 2016ZT06C322).

■ REFERENCES

(1) Wu, D.; Xu, F.; Sun, B.; Fu, R.; He, H.; Matyjaszewski, K. Design and preparation of porous polymers. *Chem. Rev.* **2012**, *112*, 3959−4015.
(2) Hsueh, H.-Y.; Yao, C.-T.; Ho, R.-M. Well-ordered nanohybrids and nanoporous materials from gyroid block copolymer templates. *Chem. Soc. Rev.* **2015**, *44*, 1974−2018.
(3) Li, C.; Li, Q.; Kaneti, Y. V.; Hou, D.; Yamauchi, Y.; Mai, Y. Self-assembly of block copolymers towards mesoporous materials for energy storage and conversion systems. *Chem. Soc. Rev.* **2020**, *49*, 4681−4736.
(4) Wang, Y. Nondestructive creation of ordered nanopores by selective swelling of block copolymers: toward homoporous membranes. *Acc. Chem. Res.* **2016**, *49*, 1401−1408.
(5) Xu, X.; Yang, Y.; Liu, T.; Chu, B. Cost-effective Polymer-based Membranes for Drinking Water Purification. *Giant* **2022**, *10*, 100099.
(6) Arora, P.; Zhang, Z. Battery separators. *Chem. Rev.* **2004**, *104*, 4419−4462.
(7) Lu, W.; Yuan, Z.; Zhao, Y.; Zhang, H.; Zhang, H.; Li, X. Porous membranes in secondary battery technologies. *Chem. Soc. Rev.* **2017**, *46*, 2199−2236.
(8) Duraikkannu, S. L.; Castro-Muñoz, R.; Figoli, A. A review on phase-inversion technique-based polymer microsphere fabrication. *Colloids Interface Sci. Commun.* **2021**, *40*, 100329.
(9) Li, S.-G.; Van den Boomgaard, T.; Smolders, C.; Strathmann, H. Physical gelation of amorphous polymers in a mixture of solvent and nonsolvent. *Macromolecules* **1996**, *29*, 2053−2059.
(10) Dong, X.; Lu, D.; Harris, T. A.; Escobar, I. C. Polymers and solvents used in membrane fabrication: a review focusing on sustainable membrane development. *Membranes* **2021**, *11*, 309.
(11) Garcia, J. U.; Iwama, T.; Chan, E. Y.; Tree, D. R.; Delaney, K. T.; Fredrickson, G. H. Mechanisms of asymmetric membrane formation in nonsolvent-induced phase separation. *ACS Macro Lett.* **2020**, *9*, 1617−1624.
(12) Guillen, G. R.; Pan, Y.; Li, M.; Hoek, E. M. Preparation and characterization of membranes formed by nonsolvent induced phase separation: a review. *Ind. Eng. Chem. Res.* **2011**, *50*, 3798−3817.
(13) Li, D.; Krantz, W. B.; Greenberg, A. R.; Sani, R. L. Membrane formation via thermally induced phase separation (TIPS): Model development and validation. *J. Membr. Sci.* **2006**, *279*, 50−60.
(14) Kesting, R. Concerning the microstructure of dry-RO membranes. *J. Appl. Polym. Sci.* **1973**, *17*, 1771−1785.
(15) Shojaie, S. S.; Krantz, W. B.; Greenberg, A. R. Dense polymer film and membrane formation via the dry-cast process Part I. Model development. *J. Membr. Sci.* **1994**, *94*, 255−280.
(16) Shojaie, S. S.; Krantz, W. B.; Greenberg, A. R. Dense polymer film and membrane formation via the dry-cast process part II. Model validation and morphological studies. *J. Membr. Sci.* **1994**, *94*, 281−298.
(17) Mandal, J.; Fu, Y.; Overvig, A. C.; Jia, M.; Sun, K.; Shi, N. N.; Zhou, H.; Xiao, X.; Yu, N.; Yang, Y. Hierarchically porous polymer coatings for highly efficient passive daytime radiative cooling. *Science* **2018**, *362*, 315−319.
(18) Cao, L.; Fu, Q.; Si, Y.; Ding, B.; Yu, J. Porous materials for sound absorption. *Compos. Commun.* **2018**, *10*, 25−35.
(19) Li, X.; Gao, J. P.; Xue, L. J.; Han, Y. C. Porous Polymer Films with Gradient-Refractive-Index Structure for Broadband and Omnidirectional Antireflection Coatings. *Adv. Funct. Mater.* **2010**, *20*, 259−265.
(20) Wong, T.-S.; Kang, S. H.; Tang, S. K. Y.; Smythe, E. J.; Hatton, B. D.; Grinthal, A.; Aizenberg, J. Bioinspired self-repairing slippery surfaces with pressure-stable omniphobicity. *Nature* **2011**, *477*, 443−447.
(21) Miller-Chou, B. A.; Koenig, J. L. A review of polymer dissolution. *Prog. Polym. Sci.* **2003**, *28*, 1223−1270.
(22) Burke, J. Solubility parameters: theory and application. *AIC The Book and Paper Group Annual*; AIC, 1984; Vol. 3, pp 13−58.
(23) Behler, K.; Havel, M.; Gogotsi, Y. New solvent for polyamides and its application to the electrospinning of polyamides 11 and 12. *Polymer* **2007**, *48*, 6617−6621.
(24) Jabbari, M.; Lundin, M.; Bahadorikhalili, S.; Skrifvars, M.; Taherzadeh, M. J. Finding solvent for polyamide 11 using a computer software. *Z. Phys. Chem.* **2020**, *234*, 517−529.
(25) Stempfle, F.; Ortmann, P.; Mecking, S. Long-chain aliphatic polymers to bridge the gap between semicrystalline polyolefins and traditional polycondensates. *Chem. Rev.* **2016**, *116*, 4597−4641.
(26) Wang, Z.; Ganewatta, M. S.; Tang, C. Sustainable polymers from biomass: Bridging chemistry with materials and processing. *Prog. Polym. Sci.* **2020**, *101*, 101197.
(27) Wang, Y.; Zhu, P.; Qian, C.; Zhao, Y.; Wang, L.; Wang, D.; Dong, X. The brill transition in long-chain aliphatic polyamide 1012: the role of hydrogen-bonding organization. *Macromolecules* **2021**, *54*, 6835−6844.
(28) Cheng, L. P.; Dwan, A. H.; Gryte, C. C. Membrane formation by isothermal precipitation in polyamide-formic acid-water systems i. Description of membrane morphology. *J. Polym. Sci. B: Polym. Phys.* **1995**, *33*, 211−222.
(29) Mao, S.; Kuldinow, D.; Haataja, M. P.; Košmrlj, A. Phase behavior and morphology of multicomponent liquid mixtures. *Soft Matter* **2019**, *15*, 1297−1311.
(30) Bae, Y.; Lambert, S.; Soane, D.; Prausnitz, J. M. Cloud-point curves of polymer solutions from thermooptical measurements. *Macromolecules* **1991**, *24*, 4403−4407.
(31) Hołda, A. K.; Vankelecom, I. F. J. Understanding and guiding the phase inversion process for synthesis of solvent resistant nanofiltration membranes. *J. Appl. Polym. Sci.* **2015**, *132*, 42130.
(32) van de Witte, P.; Dijkstra, P. J.; van den Berg, J. W. A.; Feijen, J. Phase separation processes in polymer solutions in relation to membrane formation. *J. Membr. Sci.* **1996**, *117*, 1−31.
(33) Jena, A.; Gupta, K. An innovative technique for pore structure analysis of fuel cell and battery components using flow porometry. *J. Power Sources* **2001**, *96*, 214−219.
(34) Tateno, M.; Tanaka, H. Power-law coarsening in network-forming phase separation governed by mechanical relaxation. *Nat. Commun.* **2021**, *12*, 912.
(35) Nguyen, Q. T.; Alaoui, O. T.; Yang, H.; Mbareck, C. Dry-cast process for synthetic microporous membranes: Physico-chemical analyses through morphological studies. *J. Membr. Sci.* **2010**, *358*, 13−25.

https://doi.org/10.1021/acsmacrolett.3c00086
ACS Macro Lett. 2023, 12, 697−702